Numerical simulations of natural convection in a differentially heated cubical enclosure with a partition

Toru Fusegi
Heat Transfer and Fluid Dynamics, Energy Technology Research Institute, Tokyo Gas Co. Ltd, Minato, Tokyo, Japan

Jae Min Hyun
Department of Mechanical Engineering, Korea Advanced Institute of Science and Technology, Chong Ryang, Seoul, Korea

Kunio Kuwahara
Institute of Space and Astronautical Science, Kanagawa, Japan

A high-resolution, finite-difference numerical study is made of three-dimensional natural convection in a cubical enclosure. The two vertical sidewalls of the enclosure are differentially heated. An internal partition of varying size and shape is located at the mid-plane of the cavity. Comprehensive numerical solutions to the time-dependent Navier-Stokes equations are acquired by using a control volume-based computational procedure. Two Rayleigh numbers, 10^7 and 5×10^9, are considered for the enclosure filled with air ($Pr = 0.71$). The salient three-dimensional flow characteristics are illustrated for two selected types of the partition geometry. The results clearly demonstrate the prominent three-dimensional features in the partitioned enclosure. Elaborate numerical visualization efforts have been conducted, and both the flow and thermal fields are portrayed in sufficient detail. The effects of the partition geometry on the three-dimensional flow properties are scrutinized.

Keywords: natural convection in enclosures; finite-difference method; direct numerical simulation

Introduction

Natural convection in confined spaces constitutes a central technological issue in a variety of thermal engineering systems. Applications may be found in solar energy collectors, cooling of electronic equipment, and fires in a compartment. In many of these sophisticated industrial systems, the enclosure may contain internal partitions that are partially open to allow flow passages. The presence of these internal partitions necessarily generates complicated flow fields that are time-dependent and three-dimensional (3-D) in nature. The flow characteristics of such advanced technological systems are of serious interest to both fundamental researchers and practitioners.

In the present paper, a canonical problem is proposed, and the results of 3-D numerical simulations are documented. Consider a Boussinesq fluid in a rectangular enclosure, with a solid partition (of thickness b_o) located at the mid-plane ($x^* = L_o/2$). The flow configuration and the coordinates are sketched in Figure 1. The convective flow is generated by the differential heating at the two vertical sidewalls ($x^* = 0$ and L_o). The temperatures at the left and right vertical walls are T_C and T_H, respectively, where $T_H > T_C$. The other four boundary walls of the container are considered to be thermally insulated. The overall temperature difference, $T_H - T_C$, is set equal to one tenth the average temperature, $(T_C + T_H)/2$, which is used as the reference temperature, T_o, of the present analysis. The Prandtl number of the fluid (air) is 0.71. For the actual calculations, two values of the Rayleigh number, namely, $Ra = 10^7$ and 5×10^9, are chosen to illuminate flow features at steady and unsteady states.

The partition is made of a solid material, such as a fiberglass insulation board. The centrally located rectangular opening in the partition is of height h_o (in the y-direction) and of width l_o (in the z-direction). The thickness of the partition wall is much smaller compared to the size of the enclosure ($b_o/L_o = 0.03$). In the numerical simulations, two specific examples are studied as to the precise shape of the opening in the partition. In the first example, l_o/L_o is equal to 0.4; the opening does not stretch all the way between the end walls ($z^* = 0$ and L_o), permitting fluid passages only through the doorway. This is termed Case A, for which the effect of the 3-D opening on field characteristics will be examined in detail at $Ra = 10^7$.

In the second example, l_o/L_o is set equal to 1.0, i.e., the entire bottom portion of the partition allows free passage of the fluids

Address reprint requests to Dr. Fusegi at Heat Transfer and Fluid Dynamics, Energy Technology Research Institute, Tokyo Gas Co. Ltd, 1-16-25 Shibaura, Minato, Tokyo 105, Japan.

Received 13 July 1990; accepted 30 September 1991

(Case B). The Rayleigh number of 5×10^9 is specified in order to illustrate the three-dimensionality in the field at high Ra.

The previous investigations on natural convection in an enclosure with internal partitions have not been numerous due to the presence of highly complex 3-D flow fields. Several past studies, consisting of two-dimensional (2-D) computations and experiments, of flows in a differently heated enclosure with partitions were reported in the literature.[1–10]

Experimental works have been conducted for a shallow box (the height aspect ratio of 0.5) with a partition.[1–3] High Rayleigh number ranges of about $10^9 \leqslant \mathrm{Ra} \leqslant 10^{11}$ were investigated. A centrally located partition that extended from the ceiling in a water-filled cavity was considered elsewhere[1,3] for flow visualization experiments with dye. The partition was seen to have a stabilizing effect on transitional flows near the heated wall. Flow visualization together with velocity and heat transfer measurements were undertaken[2] by using a water-filled enclosure, with a partition protruded from the floor. An extensive range of the partition aspect ratio (the ratio of the partition to the cavity height) of 0–15/16 was specified to scrutinize changes in the heat transfer rate and flow patterns. A parallel 2-D computation was carried out for the low Ra limit at Pr = 0.71. Symmetric fields with respect to the partition were predicted.

Chang et al.[4] performed a 2-D finite difference analysis of the laminar flow in an enclosure with two baffles located symmetrically at the top and bottom walls over the Rayleigh number range of $10^3 \leqslant \mathrm{Ra} \leqslant 10^8$. The soffits were found to reduce the heat transfer rate across the enclosure by approximately 20 percent when the soffits blocked one half the flow passage. The same geometries were investigated experimentally by using the Mach-Zehnder interferometry technique[5] and the laser Doppler velocimetry measurements.[6] In the former study, fluctuations were observed in the temperature fields at $\mathrm{Ra} = 10^6$; this value is considerably lower than the critical Rayleigh number for the case of a nonpartitioned enclosure with insulated horizontal walls. The increased flow resistance stemming from the existence of the baffles was cited as the cause of instability.

The problem of transient heating in an enclosure with an off-centered partition was analyzed by 2-D computations.[7] The results for a long vertical plate, which is centrally stationed in the flow field, were examined numerically.[8] In both investigations, significant variations in the field structure due to the presence of internal partitions were evident.

It is emphasized that no 3-D computations have appeared in the literature for the flow in a closed cubic cavity with partitions. On the experimental side, Scott et al.[9] and Neymark et al.[10] studied the effect of flow impediments by the partition. The media (air or water) were heated differentially by one vertical wall with a uniform heat flux, and the opposing plate was maintained at a constant temperature. A baffle with one half the enclosure height, was extended into the flow field from above in the mid-plane ($x^* = L_o/2$). The range of the flux Rayleigh number for the experiments was about 10^{11}–10^{13}. This corresponded roughly to the value of Rayleigh number of O (10^{10}), if the Rayleigh number were defined as in the present study. Random fluctuations in the fields were seen near the wall of constant heat flux.[10] In the aforementioned study,[10] a centrally located narrow opening ($l_o/L_o = 0.2$) was used. The overall heat transfer rate at the isothermal wall was calculated, and the measurements for the local temperature and velocity were conducted. The global flow patterns were visualized by using dye in a water-filled enclosure. When the l_o/L_o ratio exceeded 0.2, the Nusselt number at the cold wall was found to become insensitive to l_o/L_o.

The present investigation is implemented on a fine mesh system in order to delineate full 3-D structure of the fields. The resolution in the present 3-D simulation is comparable to that achieved in the previous 2-D analyses. The primary objective of the present study is to describe 3-D features of flow and thermal fields in the enclosure, which contains an internal partition. State-of-the-art computer simulation techniques are used to capture the salient features of the 3-D fields, which are made visible by various numerical visualization methods. The results provide quantitative information on the flows in such a complex geometry.

One area to which possible applications can be made of the present computational study is research on compartment fires. Several 3-D numerical investigations have been attempted.[11–14] In these calculations, finite-difference meshes are relatively coarse to avoid excessive CPU time and storage requirements. Compartments usually possess partial openings, which are connected to surroundings, and heat is generated by combustion at the seat of fire. There are additional complexities, which pose a great deal of difficulty in performing large-scale numerical simulations with a large number of grid points. The present enclosure problem with the well-defined boundary condition may serve as calibration cases for developing such numerical codes.

Notation

b_o, h_o, l_o	Thickness, height, and width of the partition
c_p	Specific heat at constant pressure
Fr	Froude number, u_o^2/g^*L_o
g	Gravitational acceleration
k	Thermal conductivity
L_o	Reference length (enclosure height)
p	Pressure
p_o	Reference pressure (hydrostatic pressure)
Pr	Prandtl number, $c_p^*\mu^*/k^*$
Ra	Rayleigh number, $g^*\beta^*c_p^*\rho^{*2}L_o^3(T_H - T_C)/\mu^*k^*$
Re	Reynolds number, $\rho^*u_oL_o/\mu^*$
t	Time
T	Temperature
T_o	Reference temperature, $(T_C + T_H)/2$
T_C, T_H	Cooled and heated sidewall temperatures
u_o	Reference velocity, $[g^*\beta^*L_o(T_H - T_C)]^{1/2}$
u, v, w	Velocity components in the x-, y-, and z-directions
x, y, z	Cartesian coordinates

Greek symbols

β	Thermal expansion coefficient
δ	Overheat ratio, $(T_H - T_C)/T_o$
μ	Viscosity
ρ	Density

Superscript

*	Dimensional quantities

Mathematical model

The flow is governed by the unsteady, incompressible Navier-Stokes and energy equations. The Boussinesq approximation is invoked for the fluid property variations under the assumption of a small temperature difference between the isothermal side walls ($\delta \ll 1$). The nondimensionalized form of the governing equations can be expressed in tensor notation as

$$\frac{\partial u_j}{\partial x_j} = 0 \tag{1}$$

$$\frac{\partial u_i}{\partial t} + \frac{\partial}{\partial x_j}(u_j u_i) = -\frac{\partial p}{\partial x_i} + \frac{1}{\mathrm{Re}}\frac{\partial^2 u_i}{\partial x_j \partial x_j} + \delta_{i2}\frac{T-1}{\mathrm{Fr}} \tag{2}$$

$$\frac{\partial T}{\partial t} + \frac{\partial}{\partial x_j}(u_j T) = \frac{1}{\mathrm{Re\,Pr}}\frac{\partial^2 T}{\partial x_j \partial x_j} \tag{3}$$

where δ_{ij} is the Kronecker delta ($\delta_{ij} = 1$ if $i = j$, and $\delta_{ij} = 0$ otherwise). The viscous dissipation and the pressure work terms are neglected in the energy equation.

The physical quantities are nondimensionalized in the following manner:

$$(x, y, z) = (x^*, y^*, z^*)/L_o, \qquad (u, v, w) = (u^*, v^*, w^*)/u_o$$

$$t = t^* u_o / L_o, \qquad p = (p^* - p_o)/\rho^* u_o^2, \qquad T = T^*/T_o$$

where * denotes dimensional values. The reference scales for length, velocity, pressure, and temperature are the enclosure height (L_o), the convective velocity ($u_o = [g^*\beta^* L_o(T_H - T_C)]^{1/2}$), the hydrostatic pressure (p_o), and the film temperature ($T_o = (T_C + T_H)/2$), respectively. In the present nondimensionalization (see the Notation section), the Rayleigh, Prandtl, and Reynolds numbers are related as $\mathrm{Ra} = \mathrm{Re}^2\mathrm{Pr}$.

The boundary conditions at the enclosure walls are stated as follows:

$$u = v = w = 0 \quad \text{on all the walls} \tag{4}$$

$$T = (2-\delta)/2 \quad \text{at } x = 0, \qquad T = (2+\delta)/2 \quad \text{at } x = 1$$

$$\text{and} \quad \partial T/\partial n = 0 \quad \text{at } y = 0, 1 \text{ and } z = 0, 1 \tag{5}$$

where n denotes the coordinate normal to the surface. The overheat ratio, δ, is set equal to 0.1 in the present analysis.

Solution method

A finite-difference form of the governing Equations 1–3 is obtained through a control-volume based procedure. Numerical solutions are acquired by an iterative method, together with the pressure correction algorithm, SIMPLE.[15] The present technique employs the strongly implicit procedure[16] to accelerate the convergence characteristics of the solutions. SIP is applied to the planes of constant z in order to determine simultaneously the dependent variables in the x- and y-directions on each plane.

The convection terms in the momentum Equation 2 are discretized by the QUICK methodology modified for nonuniform grids,[17] while those in the energy Equation 3 are dealt with by a hybrid scheme.[15] The QUICK scheme involves a third-order accurate upwind differencing, which possesses the stability of the first-order upwind formula and is free from substantial numerical diffusion experienced with the usual first-order techniques.

The entire enclosure is treated as the full computational domain. The number of grid points for computations is $82(x) \times 62(y) \times 62(z)$ for Case A computed at $\mathrm{Ra} = 10^7$, and $112 \times 102 \times 62$ at $\mathrm{Ra} = 5 \times 10^9$ for Case B. Variable grid spacing is introduced to resolve steep gradients of the velocity and the temperature near the walls. For the region occupied by the solid partition, the velocities are set equal to zero throughout the computations. The ratio of the thermal conductivity of the solid material of the partition (soffit) to that of the fluid (air) is 1.5. The discontinuity of the thermal conductivities in the flow domain and in the soffit is handled by evaluating the interfacial conductivity with a harmonic mean.[15]

An implicit method is used to march the unsteady solutions in time. Convergence of computations at each time step is declared when the following criterion is met:

$$\frac{|\phi_n - \phi_{n-1}|}{|\phi_n|_{maximum}} \leqslant 10^{-4} \quad \text{for all } \phi \tag{6}$$

where ϕ indicates any dependent variable, and n refers to the value of ϕ at the n^{th} iteration level.

The numerical method of the present study is identical to that applied previously to an analysis of natural convection in a differentially heated 3-D nonpartitioned cubical enclosure.[18] The reference documented a procedure to obtain grid-independent 3-D solutions with nonuniform meshes consisting of 62^3 grid points in a range of $10^3 \leqslant \mathrm{Ra} \leqslant 10^6$. The reader should consult the reference[18] for detail; it is summarized as follows. Parallel 2-D computations (in x-y coordinates) were conducted, in which the mesh spacing was altered systematically until close agreement with a reliable solution (such as a bench mark solution[19]) was reached. This grid network was used to construct 3-D counterparts. This method was adopted since extension of a well-defined technique for a uniform grid system[20] to nonuniform meshes was not obvious. Basically the same procedure is employed in the present study. In addition, one computation was performed for the case of a nonpartitioned enclosure of $\mathrm{Ra} = 10^7$ by doubling the number of grid points in the x-direction. Changes in the peak velocity were found to be less than 2 percent, indicating that 62 mesh points would be sufficient. For Case A, which deals with a doorway in the central plate, fine meshes are distributed in the vicinity of the opening to properly resolve 3-D flows present in the region (Figure 1b).

Results and discussion

Computations were run on a Hitachi S-820/80 supercomputer system at ICFD. The system has a maximum CPU speed of 3 Gflops and a maximum incore memory of 512 MB. Three-dimensional field data is presented in this section by means of various numerical visualization techniques. The 3-D graphics were produced by interactive graphic software modules,[21] which are implemented in a Fujitsu VP-200 supercomputer system at ICFD.

Case A at Ra = 10^7

The computation for Case A (the geometry of the opening in the partition is described as $l_o/L_o = 0.4$, $h_o/L_o = 0.5$, and $b_o/L_o = 0.03$) was performed at the Rayleigh number of 10^7; the steady-state solution was reached. Figure 2 illustrates the perspective views of the temperature and flow fields represented by isotherms and isovorticity surfaces, respectively. Due to the presence of the partition with the opening, three-dimensionalities (z-variations in the fields) are prominent. Since the opening is located near the bottom wall, the sinking motion of the cold fluid originating from the cooled sidewall ($x = 0$) can find its

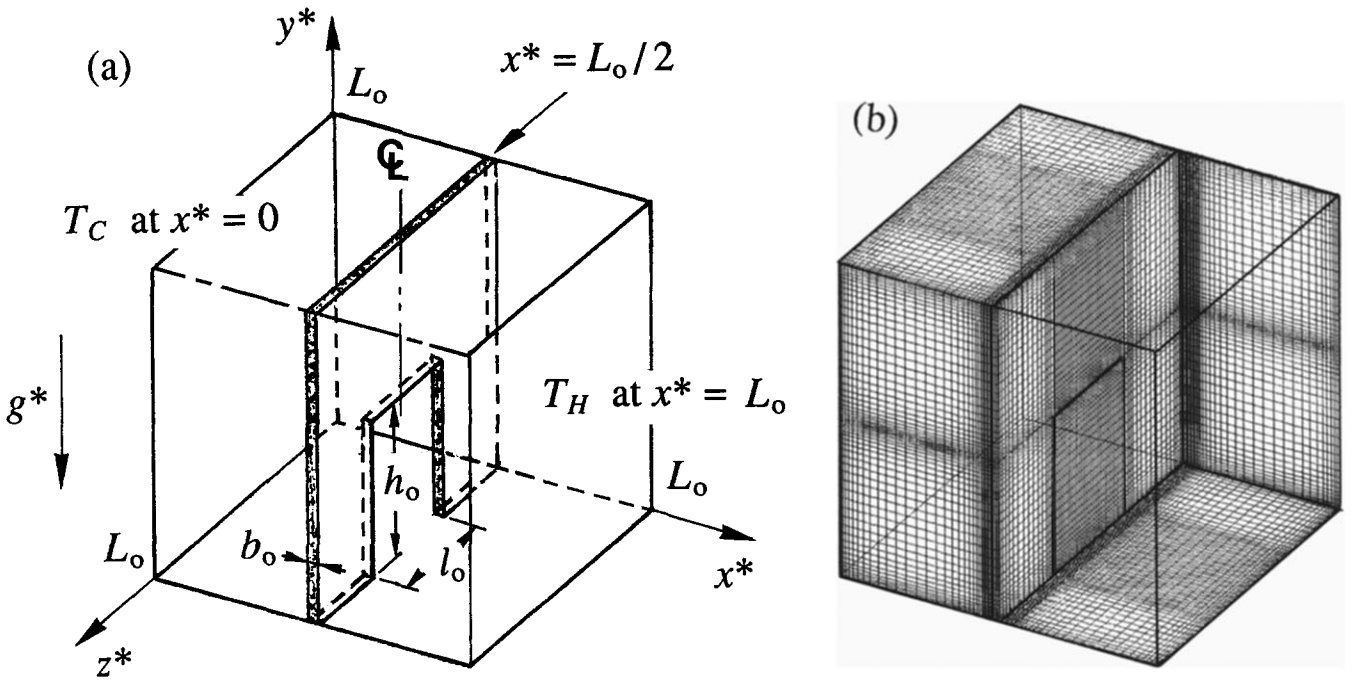

Figure 1 The schematics of the cubical enclosure. (a) The geometry and the boundary conditions (the planes located at $y^* = L_o$ and $z^* = L_o$ are removed to show the enclosure interior); (b) finite-difference grid network

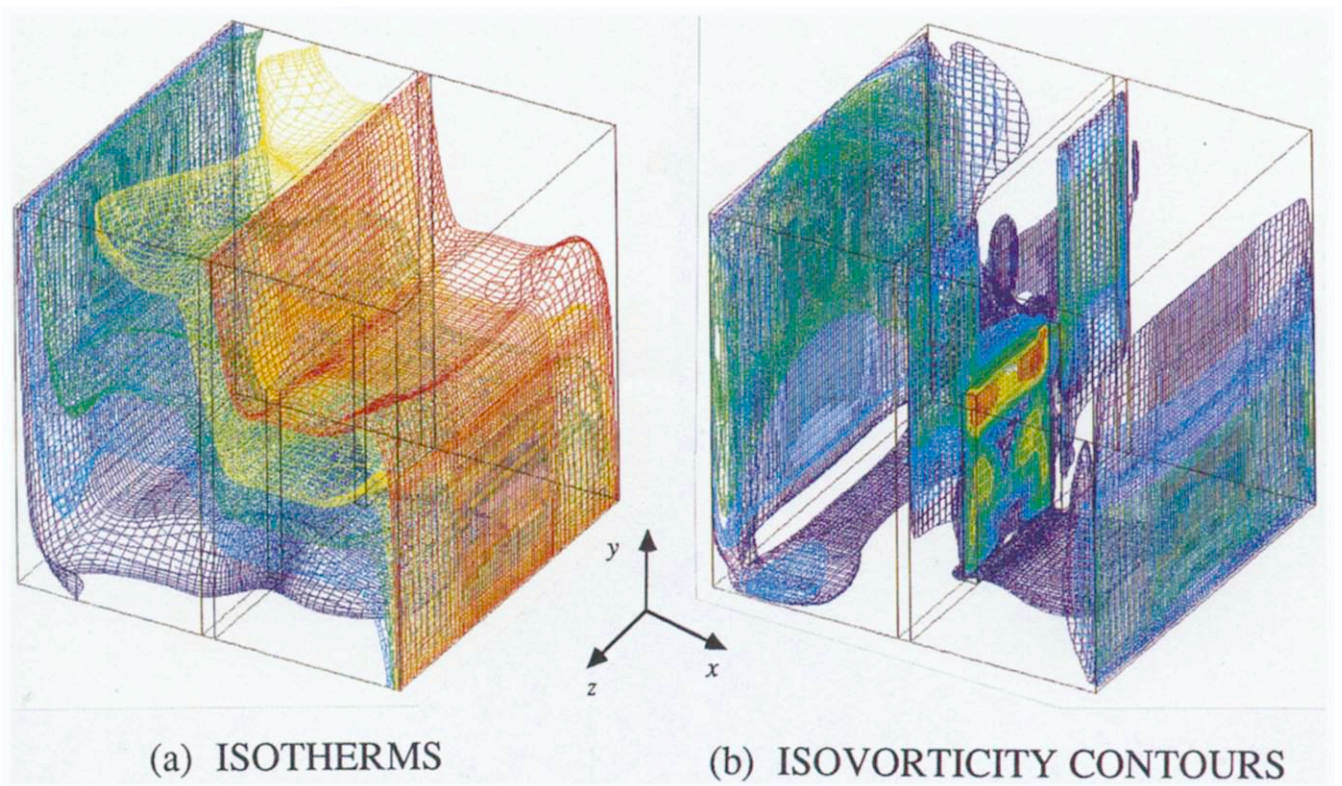

Figure 2 The isotherms and the isosurfaces of the absolute values of the vorticity inside the cube (Case A) [(contour levels) isotherms: 0.9667 (dark blue), 0.9833 (blue), 1.0 (green), 1.017 (yellow), 1.033 (red); isovorticity surfaces: 5.0 (dark blue), 10.0 (blue), 20.0 (green), 50.0 (yellow), 80.0 (red)]

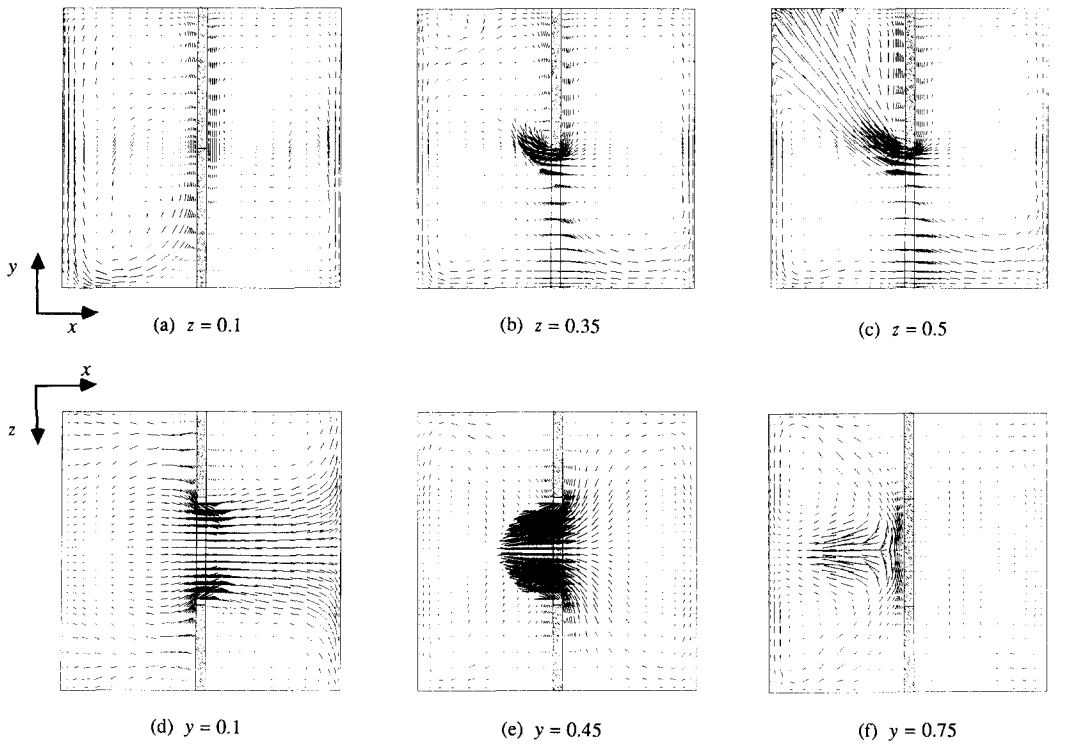

Figure 3 Velocity vectors projected on various planes located at constant y and z (Case A)

way along the bottom surface. Therefore, the downward flow near the cooled sidewall is vigorous. On the other hand, near the heated sidewall ($x = 1$), the hot fluid moves upward; however, this flow is blocked by the partition in the upper portion of the enclosure. Consequently, this heated fluid occupies a near-stagnant region in the upper-level compartment between the partition and the heated sidewall. The warm fluid piles up in this near-stagnant region, and the temperature of this area is close to that of the heated sidewall.

Away from the boundary layers, which develop in the proximity of the isothermal sidewalls and the partition, the vertical temperature distribution inside the enclosure can be characterized by a two-zone structure. This has been observed in the core of the partitioned enclosures.[10] The two zones consist of the lower temperature part (the cold zone) in the left half of the flow field ($0 < x < 0.5$) and the higher temperature part (the hot zone) in the right half ($0.5 < x < 1.0$). In the flow field, extremely high concentration of the vorticity is discernible near the upper corners of the doorway.

The projected velocity vectors in various cross-sectional planes are depicted in Figure 3. In the areas near the sidewall (Figure 3a for $z = 0.1$), the flow domain is completely divided into two regions by the partition. Figures 3b and c illustrate the velocity vectors in two different vertical planes, which include the aperture. In both cases, the strongly buoyant flow generated near the heated vertical sidewall ($x = 1$) descends in the heated plate side of the partition and is discharged into the cold zone by turning its direction sharply along the bottom part of the partition. As shown in Figure 3c, near the symmetry plane ($z = 0.5$), the flow behaves like a jet impinging toward the upper left corner of the enclosure. This jet-like flow is absent in Figure 3b, which conveys flow features in a constant z-plane near the edge of the partition opening. Remarkable z-variations of the flow are exhibited in these two figures.

The flow of cold fluid, which is directed toward the hot from the cold zones in the lower part of the enclosure ($y = 0.1$), is portrayed in Figure 3d. Due to the contraction of the flow passage by the soffit, a significant increase in the flow intensity across the aperture is clearly seen. The hot fluid, which flows in the opposite direction in the uppermost portion of the doorway ($y = 0.45$), is displayed in Figure 3e. In the region far above the opening ($y = 0.75$), the jet in the cold zone and the reverse flow formed between the jet in the center and the end planes ($z = 0$ and 1) are clearly visible in Figure 3f. Again, prominent z-variations are apparent in these cross-sectional views of the velocity field.

The heat transfer rate (the overall Nusselt number; see Equation 7 for its definition) at the isothermal walls is calculated to be 13.2, which implies approximately a 15 percent reduction of the value for the nonpartitioned enclosure for which $Nu_{overall}$ is equal to 15.4. An additional computation has been made by extending the opening width to the enclosure length (i.e., $l_o = L_o$). The flow patterns (not shown) are different from those reproduced in Figure 3, except at $z = 0.5$, due to a broader opening. The z-variation of the flow field is weak, indicating that the two-dimensionality prevails. The overall Nusselt number, which is found to be 14.0, shows only a slight reduction from the result for the nonpartitioned cavity.

From these observations, the narrow opening is seen to generate notable 3-D flows in the present case.

Case B at Ra = 5 × 10⁹

For comparison purposes, results of a parallel 2-D computation for Case B are included in the present discussion. The identical geometric parameters to those for the 3-D partition were adopted ($h_o/L_o = 0.5$ and $b_o/L_o = 0.03$). The Rayleigh number

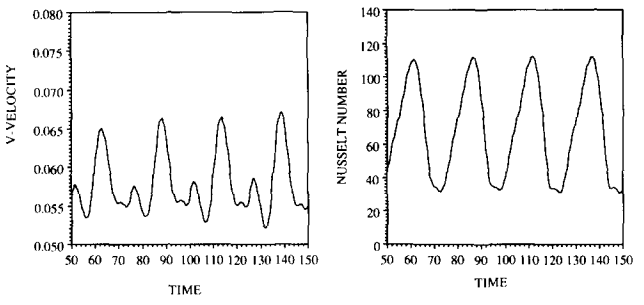

(a) VERTICAL VELOCITY AT (x, y) = (0.01, 0.25)

(b) OVERALL NUSSELT NUMBER AT THE MID-PLANE LOCATED AT x = 0.5

Figure 4 Time histories of the local velocity and the overall Nusselt number (Case B, 2-D results)

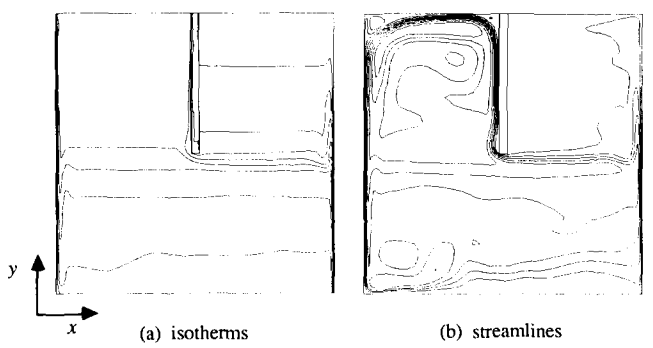

(a) isotherms (b) streamlines

Figure 5 The time-averaged isotherms and stream-function contours (Case B, 2-D results) [increments of contours: (a) 0.01; (b) 0.58×10^{-3}]

for the present case is set equal to 5×10^9. A nondimensional time step of 0.01 is used for the computations. The minimum spacing of the nonuniform finite-difference mesh is approximately 8×10^{-4} (nondimensional length), which occurs near the isothermal walls and in the immediate vicinity of the opening.

The critical Rayleigh number for transition to turbulence in this configuration does not appear to be known. In the case of 2-D, nonpartitioned differentially heated square cavity, oscillatory flow is detected at around $Ra = 2 \times 10^8$.[22,23]

Figure 4 exemplifies the time histories of the vertical velocity (v) inside the heated-wall boundary layer and of the overall Nusselt number in the mid-x plane ($x = 0.5$) for 2-D computations. The nondimensional heat transfer rate (the overall Nusselt number, $Nu_{overall}$) at this plane is defined as

$$Nu_{overall} = -\int_0^1 \frac{\partial T}{\partial x}(x = 0.5, y)\, dy + Re \cdot Pr \int_0^1 u[T(x = 0.5, y) - 1]\, dy \qquad (7)$$

At this high Rayleigh number, convection is predominant, and the first term in the right-hand side of Equation 7 is negligibly small. Regular periodic oscillations are discernible in the flow and temperature fields, as displayed in Figure 4. The period of the large-scale fluctuations appears to be approximately 25 (in the nondimensional time) in the present result.

The sequential data over a time interval of 100 were averaged. The temporally averaged isotherms and stream function contours are presented in Figure 5. The entire flow field is thermally stratified, and very thin thermal and hydrodynamic boundary layers are seen to develop near the isothermal walls. The boundary layer on the heated sidewall penetrates up to only the mid-height of the enclosure; the buoyant flow cannot move through the stratified upper-right region beyond that height. Around this level, the boundary layer separates from the surface and turns perpendicular to the wall. As it reaches the bottom portion of the partition, the flow again makes a turn and climbs up the cooled plate side of the baffle. The flow path follows the profiles of the inner horizontal and vertical sidewalls. The recirculation zones are seen at the corners. This flow pattern exhibits a drastic difference from that of Case A discussed in the previous subsection. It is recalled that for Case A, a jet-like flow is formed in the diagonal direction across the upper-left portion of the cold zone.

The root mean squares and cross-correlation of the fluctuating components are computed and displayed in Figure 6. These correlations are defined as

$$\overline{\phi_i' \phi_j'} = \frac{1}{\Delta t} \int_{t_o}^{t_o + \Delta t} \phi_i' \phi_j'\, dt \qquad (8)$$

where ϕ_i' denotes the fluctuating component of any variable, t_o stands for the reference time level, and Δt represents the time interval. In all the fields presented in Figure 6, high concentrations of the correlations are notable in the areas where the mean flow is vigorous. The temperature correlations are seen to be several orders of magnitude lower than those for the velocity correlations.

An instantaneous 2-D field at this Rayleigh number is used as the initial condition, and a 3-D computation is carried out. Calculations are continued until the effect of the initial condition becomes negligible in the entire field, which occurred at approximately 4000 time steps. The total CPU time takes

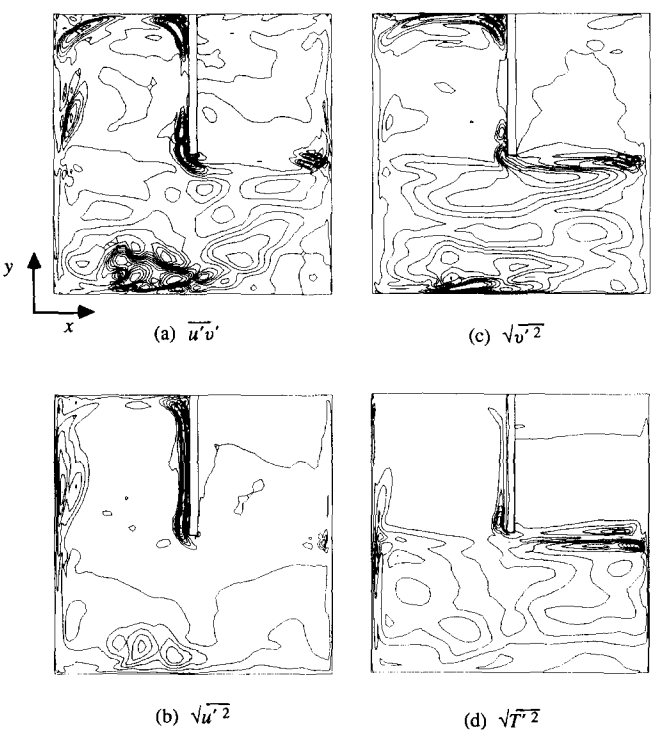

(a) $\overline{u'v'}$ (c) $\sqrt{v'^2}$

(b) $\sqrt{u'^2}$ (d) $\sqrt{T'^2}$

Figure 6 The cross-correlation and root mean squares of the fluctuation components (Case B, 2-D results) [increments of contours: (a) 0.5×10^{-4}; (b) 0.5×10^{-3}; (c) 0.4×10^{-4}; (d) 0.5×10^{-4}]

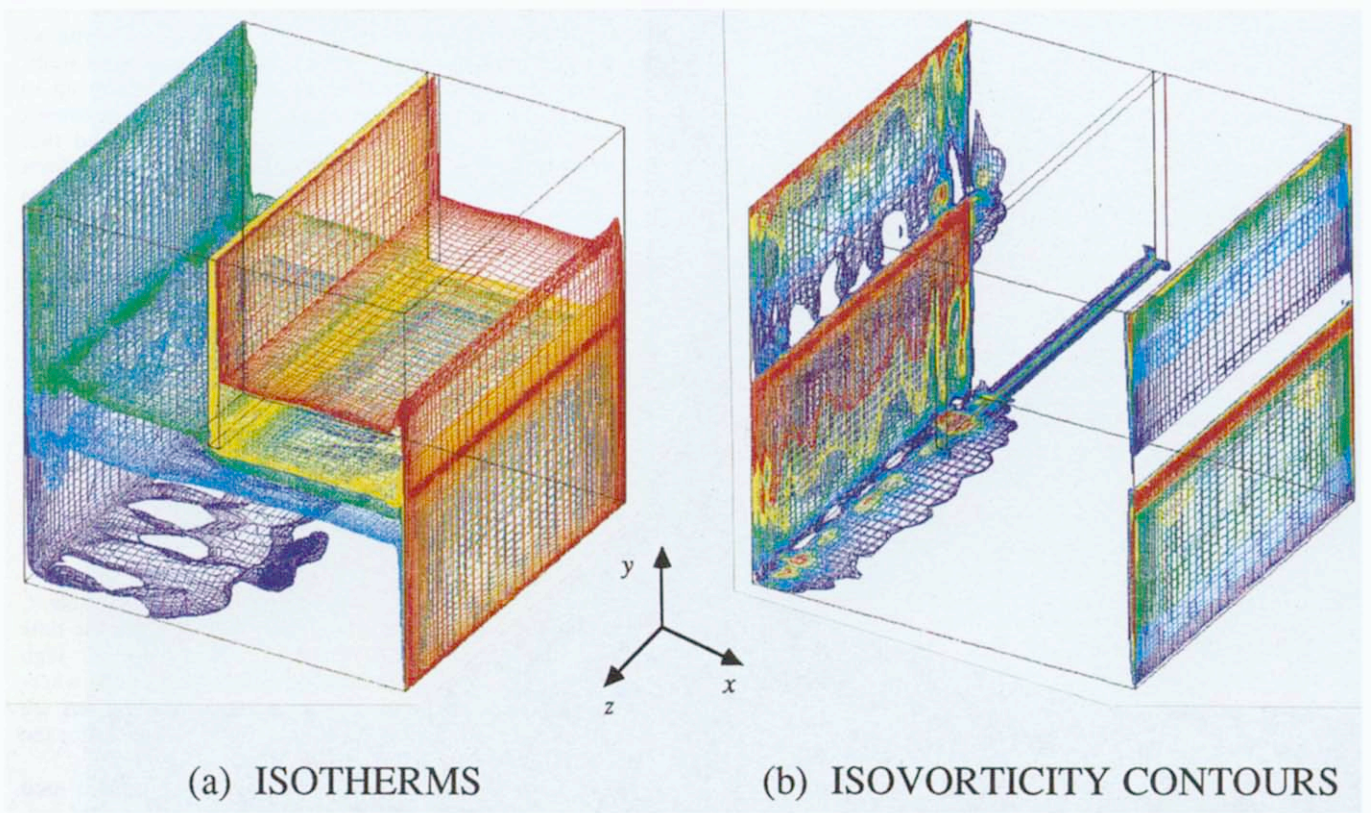

Figure 7 Instantaneous temperature and absolute vorticity fields (Case B, 3-D results) [(contour levels) isotherms: 0.9667 (dark blue), 0.9833 (blue), 1.0 (green), 1.017 (yellow), 1.033 (red); isovorticity surfaces: 20.0 (dark blue), 40.0 (blue), 60.0 (green), 80.0 (yellow), 100.0 (red)]

about 80 hours on the Hitachi S820/80 supercomputer. This placed an extremely severe requirement for the computational resources; therefore, it was not practically possible to obtain data of a one full period of the field fluctuations, for which 2500 more time step calculations would have been needed.

Figure 7 illustrates perspective views of the instantaneous temperature and absolute vorticity fields. The overall isotherm patterns look similar to the time-averaged 2-D results, which were shown in Figure 5. However, substantial z-variations are discernible in the temperature field in the lower-left portion of the enclosure. These three-dimensionalities are in evidence in the fluids of low temperature. These irregular patterns change shapes as time progresses. In the vorticity field, high concentration of the vorticity takes place within very thin layers adjacent to the isothermal walls and the bottom part of the partition. In both fields, the overall features are substantially similar to those of 2-D results in the regions away from the two end plates ($z = 0$ and 1); thus, the 2-D approximation of the field structure appears to be reasonable in the bulk of the fluid.

Conclusions

The two types of the geometry of the internal openings were considered to reveal the 3-D characteristics of natural convection flow in a differently heated cubical enclosure with a centrally located partition. In Case A (partial opening), the flow field is divided into two zones by the partition. The patterns of the thermal stratification in each zone differ significantly due to the partition geometry, which allows flow passage only through the lower half of the enclosure. An impinging jet flow across the opening (doorway) is observed near the centerline in the upper-half region of the cold zone. The considerable three-dimensionalities of the flow are attributed mainly to the presence of the partition. At $Ra = 10^7$, the flow appeared to be laminar.

In contrast, the flow exhibits steady periodic oscillations in Case B, in which the opening extends all the way between the end walls ($z = 0$ and 1). In this case, the Rayleigh number is increased to 5×10^9. Examination of the instantaneous fields displays strong local z-variations, although in the bulk of the flow field the 2-D approximation is largely valid. The dominant flow is seen to be directed along the solid walls. High concentration of the correlations is evident in these regions, indicating that they are the possible sources to generate unsteady flows.

Acknowledgment

The authors are very grateful to the Institute of Computational Fluid Dynamics (ICFD) for generous use of its supercomputing resources.

References

1 Nansteel, M. W. and Greif, R. Natural convection in undivided and partially divided rectangular enclosures. *J. Heat Transfer*, 1981, **103**, 623–629

2 Lin, N. N. and Bejan, A. Natural convection in a partially divided enclosure. *Int. J. Heat Mass Transfer*, 1983, **26**, 1867–1878

3 Nansteel, M. W. and Greif, R. An investigation of natural convection in enclosures with two- and three-dimensional partitions. *Int. J. Heat Mass Transfer*, 1984, **27**, 561–571

4 Chang, L. C., Lloyd, J. R. and Yang, K. T. A finite difference study of natural convection in complex enclosures. *Proc. 7th Int. Heat Transfer Conf.*, Vol. 2, 1982, 183–188

5 Bajorek, S. M. and Lloyd, J. R. Experimental investigation of natural convection in partitioned enclosures. *J. Heat Transfer*, 1982, **104**, 527–532

6 Bilski, S. M., Lloyd, J. R. and Yang, K. T. An experimental investigation of the laminar convection velocity field in square and partitioned enclosures. *Proc. 8th Int. Heat Transfer Conf.*, Vol. 4, 1986, 1513–1518

7 Fu, W.-S., Perng, J. C. and Shieh, W.-J. Transient laminar natural convection in an enclosure partitioned by an adiabatic baffle. *Numer. Heat Transfer*, 1989, **16**, 325–350

8 Kelkar, K. M. and Patankar, S. V. Numerical prediction of natural convection in partitioned enclosures. *Natural Convection in Enclosures—1986*, ASME HTD **63**, 63–71

9 Scott, D., Anderson, R. and Figliola, R. Blockage of natural convection boundary layer flow in a multizone enclosure. *Int. J. Heat and Fluid Flow*, 1988, **9**, 208–215

10 Neymark, J., Boardman, C. R., Kirkpatrick, A. and Anderson, R. High Rayleigh number natural convection in partially divided air and water filled enclosures. *Int. J. Heat Mass Transfer*, 1989, **32**, 1671–1679

11 Bagnaro, M., Laouisset, M. and Lockwood, F. C. Field model prediction of some room fires: Steady and transient. *Fire Dynamics and Heat Transfer* (J. G. Quintiere, et al., Eds.), ASME HTD, 1985, **25**, 107–114

12 Cox, G., Kumar, S. and Markatos, N. C. Some field model validation studies. *Proc. 1st Int. Symp. in Fire Safety Science*, 1985, 159–172

13 Markatos, N. C. and Pericleous, K. A. An investigation of three-dimensional fires in enclosures. *Fire Dynamics and Heat Transfer* (J. G. Quintiere, et al., Eds.), ASME HTD, 1985, **25**, 115–124

14 Satoh, K. Three-dimensional field model analysis of fire-induced flow in an enclosure with a doorway opening—Comparison with NBS fire tests. *Report Fire Research Inst. of Japan*, 1985, **60**, 53–63

15 Patankar, S. V. *Numerical Heat Transfer and Fluid Flow*. Hemisphere Publishing, Washington, DC, 1980

16 Stone, H. L. Iterative solution of implicit approximations of multi-dimensional partial differential equations. *J. Numer. Analy.*, 1968, **5**, 530–558

17 Freitas, C. J., Street, R. L., Findikakis, A. N. and Koseff, J. R. Numerical simulation of three-dimensional flow in a cavity. *Int. J. Numer. Methods in Fluids*, 1985, **5**, 561–575

18 Fusegi, T., Hyun, J. M., Kuwahara, K. and Farouk, B. A numerical study of three-dimensional natural convection in a differentially heated cubical enclosure. *Int. J. Heat Mass Transfer*, 1991, **34**, 1543–1557

19 de Vahl Davis, G. Natural convection of air in a square cavity: A bench mark numerical solution. *Int. J. Numer. Methods Fluids*, 1983, **3**, 249–264

20 Churchill, S. W., Chao, P. and Ozoe, H. Extrapolation of finite-difference calculations of laminar natural convection in enclosures to zero grid size. *Numer. Heat Transfer*, 1981, **4**, 39–51

21 Shirayama, S. and Kuwahara, K. Patterns of three-dimensional boundary layer separation. *25th Aerospace Sciences Meeting*, AIAA Paper 87-0461, 1987

22 Paolucci, S. and Chenoweth, D. R. Transition to chaos in a differentially heated vertical cavity. *J. Fluid Mech.*, 1989, **201**, 379–410

23 Henkes, R. A. W. M. and Hoogendoorn, C. J. On the stability of the natural convection flow in a square cavity heated from the side. *Appl. Sci. Res.*, 1990, **47**, 195–220